analytical chemistry

pubs.acs.org/ac Article

High-Throughput Mass Spectrometry Screening Platform for Discovering New Chemical Reactions under Uncatalyzed, Solvent-Free Experimental Conditions

Dmytro S. Kulyk, Enoch Amoah, and Abraham K. Badu-Tawiah*

Cite This: *Anal. Chem.* 2020, 92, 15025−15033 Read Online

ACCESS | Metrics & More | Article Recommendations | Supporting Information

ABSTRACT: A gas-phase high-throughput reaction screening platform was developed for the first time to study chemical structures of closely related functional groups and for the discovery of novel organic reaction pathways. Experiments were performed using the contained atmospheric pressure chemical ionization (APCI) source that enabled nonthermal, nonequilibrium plasma chemistry to be monitored by mass spectrometry (MS) in real time. This contained-APCI MS platform allowed an array of reagents to be tested, resulting in the studies of multiple gas-phase reactions in parallel. By exposing headspace vapor of the selected reagents to corona discharge, solvent-free Borsche−Drecsel cyclization reaction, Katritzky chemistry, and Paal−Knorr pyrrole synthesis were examined in the gas phase, outside the high vacuum environment of the mass spectrometer. A new radical-mediated hydrazine coupling reaction was also discovered, which provided a selective pathway to synthesize secondary amines without using a catalyst. The mechanisms of these atmospheric pressure gas-phase reactions were explored through the direct capture of intermediates and via comparison with the corresponding bulk solution and droplet-phase reactions.

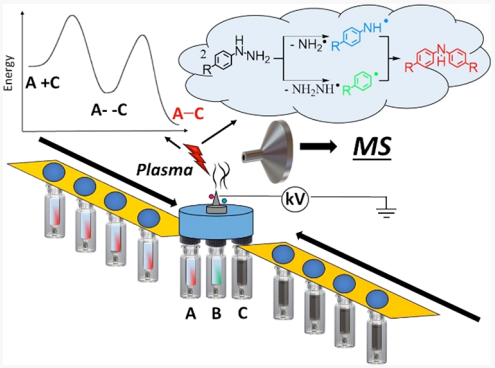

INTRODUCTION

High-throughput experimentation (HTE) enables a large number of experiments to be conducted in parallel through systems automation. The process is very well developed for bioassays[1−3] but less so for chemical reaction screening. We report here the first gas-phase high-throughput experiment for chemical reaction screening under ambient conditions. Biochemical experiments are often performed in an aqueous medium and at (or near) room temperature so HTE implementation is straightforward. Chemical reactions, on the other hand, are carried out in different solvents and in a broad temperature range. The use of volatile organic solvents brings further complications in terms of material compatibility and evaporative loss, all making it even more challenging to automate the HTE process for chemical reactions. Therefore, the ability to perform chemical reactions in a solvent-free environment, at room temperature, and pressure may represent a unique opportunity to increase the speed with which new chemical reactions can be screened.

Recently, the use of desorption electrospray ionization (DESI) in HTE has alleviated some of the difficulties associated with engineering microarrays for chemical reaction screening through the integration of sample introduction, reaction, and analysis of products into a single mass spectrometry (MS) experimental step.[4,5] The presence of evaporating charged microdroplets in DESI allows the confinement of reactants in smaller volumes, leading to concentration, surface, and pH effects that have been found to collectively increase reaction rates.[6−9] The purpose of DESI high-throughput screening has remained the rapid optimization of solution-phase reaction conditions; it is rarely used for high-throughput discovery of new reactions. The gas-phase HTE platform described in this study is not only capable of reproducing known solution-phase reactions but it also allows new organic reaction discovery. In general, the complete absence of solvent makes gas-phase reactions very efficient and fast. Despite this promise, gas-phase reactions are not a common tool in most analytical laboratories. This is because gas-phase ion/molecule and ion/ion reactions require substantial modification to the mass spectrometer, which limits their widespread use.

Like solution-phase experiments, reported gas-phase HTE mimics have also focused on the development of standard workflows for targeted proteomic assays.[10] For example, the most widely used gas-phase reaction is electron transfer

Received: July 11, 2020
Accepted: October 21, 2020
Published: November 5, 2020

https://dx.doi.org/10.1021/acs.analchem.0c02960
Anal. Chem. 2020, 92, 15025−15033

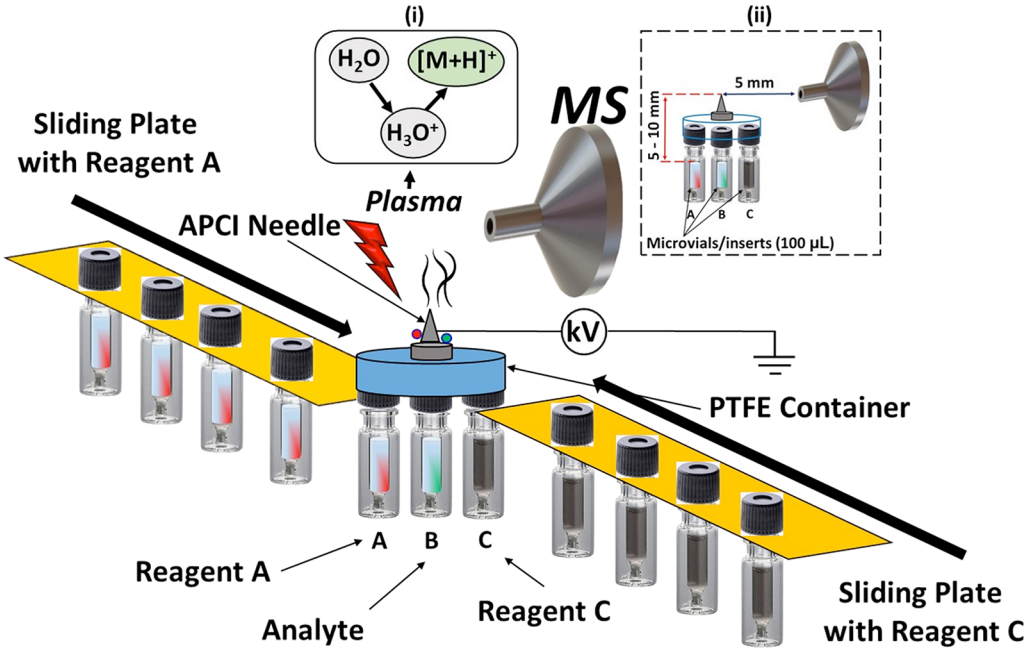

Figure 1. Schematic of the contained-APCI MS screening platform. Containers (A, B, and C) can be filled (<100 μL) with different reagent combinations (A and C) and analyte (B), and robotically or manually exposed to corona discharge (red thunder) by sliding plates. Headspace vapor or electrostatically attracted particles of reagents react with each other in the gas-phase upon plasma initiation through the application of high direct current (DC) voltage (4−6 kV) to the stainless steel needle. Detection of reaction products is conducted by mass spectrometry in real time. Insert (i) illustrates plasma-based ion/molecule reaction, leading to analyte (M) ionization to give $[M + H]^+$ ions. Insert (ii) is the zoomed-in region of the PTFE container relative the mass spectrometer, showing distances between MS inlet, microvials containing samples, and APCI needle.

dissociation, which enables high-throughput liquid chromatographic tandem MS (MS/MS) analysis for rapid top-down protein identification using commercially available ion trap mass spectrometers.[11−13] The fundamental experiments in this field include the concentration of ion current through ion/ion reactions (in a so-called ion packing process) to improve analytical sensitivity.[14] Ozone-induced dissociation is another relevant gas-phase reaction that has enabled positional isomers and the stereochemistry of unsaturated fatty acids and lipids to be determined in a high-throughput fashion.[14−16] Gas-phase ion/molecule reactions are also extremely powerful in providing detailed structural information for unknown compounds, including the type and number of different functionalities present in the compound.[17] Notice that all these gas-phase reactions are performed inside the high vacuum environment of the mass spectrometer, something that limits access to analyte, and thus reducing the overall throughput of the experiment. Also, determination of the chemical structure has been the ultimate objective for these conventional gas-phase ion/molecule and ion/ion reactions. The proposed gas-phase HTE platform is unique in that it operates at atmospheric pressure, outside the high-vacuum environment of the mass spectrometer, and it is capable not only for structural determination but also for the discovery of new organic reaction pathways. Most importantly, the platform is applicable for screening both volatile and nonvolatile analytes without heating and with no need for an external catalyst, which results in gas-phase organic reactions in a solvent-free environment.

The motivation for creating atmospheric pressure MS-based gas-phase HTE platform is fourfold: (1) possible application in drug design and discovery to facilitate rapid prediction of molecular structure and physicochemical properties; (2) to enable direct analysis without sample preparation. Given that there are approximately 10^{60} drug-like pharmaceutically perspective molecules employed in drug discovery,[18] the speed and ease of operation of reaction screening becomes critical parameters in HTE. MS-based analytical platforms show great potential in this respect,[19−23] but almost all reported methods require sample preparation and optimization of several solution-phase parameters (e.g., solvent, pH, and temperature), which significantly increases the analysis time. (3) To facilitate smaller sample consumption (<*n*mol/min)[24,25] during HTE, this objective is achieved via the use of headspace vapors or electrostatically attracted particles from volatile and nonvolatile reagents, respectively; (4) to enable highly efficient and sensitive detection for a variety of analyte types (polar, nonpolar, volatile, and nonvolatile), which can be uniquely suited for the detection of reaction intermediates with different chemical structures.

There is a substantial literature on the use of nonthermal plasmas generated by electrical discharge at atmospheric pressure in chemical synthesis.[26−28] This research area is particularly attractive because plasmas can be powered by intermittent electricity generated from renewable sources such as solar and wind, thus incorporating valuable chemical synthesis into a renewable carbon cycle that can reduce dependence on fossil fuels. An important feature about plasma chemistry is that large quanta of energy can be transferred to a reactant in a single excitation event, making it possible to access higher excited states. Aspects of our previous research have focused on the use of photons to generate excited-state species for reactions in microdroplets,[29,30] but this requires photosensitizers whose redox potential match that of the analyte(s) of interest. This limits the general utility of associated analytical photoreaction screening methods. Since electron collisions in plasma do not depend on chromophoric groups or sensitizers, we anticipated that a screening platform

https://dx.doi.org/10.1021/acs.analchem.0c02960
Anal. Chem. 2020, 92, 15025−15033

based on plasma should make it possible to excite all kinds of molecules.

Therefore, we created a novel contained-atmospheric pressure chemical ionization (contained-APCI, Figure 1) source for high-throughput gas-phase reaction screening using nonequilibrium plasma chemistry. The contained-APCI platform is capable of screening up to two chemical reactions in parallel for the array of reagents (e.g., monitoring of reaction between reagents A and B vs reagents B and C, where B is the analyte). The array of reagents to be reacted against the analyte B is delivered by a sliding plate. To minimize secondary effects from reactive oxygen species generated from atmospheric gases, we designed the contained-APCI screening platform to have a short path length (<5 mm), leading to short residence time (<5 s) of reagents in the plasma. This was achieved by introducing reactants in the form of headspace vapors (or particles released into air via electrostatic attraction due the proximal DC voltage)[24] in the open laboratory environment. To increase ease of operation, the platform was further simplified by not using external gases for plasma generation. Plasma species generated with the assistance of N_2 gas are known to be more energetic and reactive compared with O_2.[31] This implies that although the terminal active reagent ions in APCI typically involve protonated water clusters $H^+(H_2O)_n$,[32,33] analyte's internal energy deposition can be controlled by the type of nebulizer gas used. Hence, by employing ambient air as discharge gas, we expect to further decrease secondary effects.

We applied the optimized contained-APCI platform to study gas-phase Borsche−Drecsel cyclization reaction, Katritzky chemistry, and Paal−Knorr pyrrole synthesis, all in a solvent-free environment. Through the careful selection of these known reactions, we showcased for the first time the ability to differentiate closely related functional groups (e.g., amines vs hydrazine) through gas-phase ambient reactions. Screening of multiple reagents (5 total) against a selected 2-butanone reactant and subsequent real-time product detection was accomplished in less than 60 s. The contained-APCI screening platform also enabled the discovery of a new radical mediated gas-phase hydrazine coupling reaction, which afforded a facile pathway to selectively synthesize secondary amines. Finally, mechanistic insights were sought through the direct capture of intermediates and comparison of selected gas-phase reactions to the corresponding bulk solution and droplet-phase reactions.

EXPERIMENTAL SECTION

Contained-APCI Platform. In its full operational form, the contained-APCI reaction screening platform (Figure 1) comprised of a PTFE container with a closed top and open bottom (4 cm L × 2 cm W × 0.5 cm H) in which three independent 100 μL glass microvials A, B, and C can be inserted for sample introduction. Reagents in the two of the glass microvials (A and C) can be interchanged via a sliding plate containing other microvials, allowing a series of reactions to be monitored simultaneously. The only outlet (ID, 5 mm) for all three inputs is located at the top of the PTFE container. The stainless steel APCI needle is placed adjacent to this single outlet, allowing gas-phase reaction and ionization to be initiated upon the application of DC voltage. Because the condensed-phase sample (100 μL) is contained in a microvial and analyzed through a noncontact means (i.e., there is no direct contact between the sample and APCI needle), our technique is safe to operate, minimally destructive, and enables the sample to be reanalyzed by different analytical methods.[1−3] Headspace vapors and particles of nonvolatile solid reagent are supplied through the outlet toward the inlet of the mass spectrometer. Upon the application of high DC voltage (4−6 kV) to the stainless steel APCI needle, invisible corona discharge (no sparking at optimized distances used) is induced in the vicinity of the outlet, allowing brief exposure of the gas-phase analyte to the plasma and initiating instantaneous solvent-free chemical reactions and ionization at ambient pressure and temperature. Sliding plates in their turn allow an array of reagents to be introduced rapidly for high-throughput reaction monitoring. The ability of the contained-APCI platform to ionize a broad range of reagents with markedly different physicochemical properties (volatility, polarity, basicity, and acidity, etc.) makes this device particularly effective for studying various gas-phase reactions using mass spectrometry. The characterization of the ionized reaction products and intermediates was achieved in real time using both tandem MS and exact mass measurements.

Mass Spectrometry. Reaction systems were analyzed by a Thermo Fisher Scientific Velos Pro LTQ and LTQ Orbitrap (for high-resolution data) mass spectrometers (San Jose, CA, USA). Unless otherwise stated, MS parameters employed were as follows: 400 °C capillary temperature, 4−6 kV spray voltage, 5 mm distance between the tip of the APCI needle and microvial containing the analyte, 5 mm distance from the tip of APCI needle to MS inlet, 3 microscans, 100 ms ion injection time, and 60% S-lens voltage for Velos Pro LTQ and 55 V tube lens voltage for LTQ Orbitrap. Spectra were recorded for at least 30 s, yielding an average of 300 individual scans. Thermo Fisher Scientific Xcalibur 2.2 SP1 software was utilized for MS data collecting and processing. Unless otherwise mentioned, tandem MS with collision-induced dissociation (CID) was performed for analyte identification. Thirty percent (manufacturer's unit) and 1.5 Th (mass/ charge units) for isolation window of normalized collision energy were selected for the CID tests.

Reactions in Bulk and Droplet Media. All reaction mixtures presented here for solution and droplet chemistry were prepared in acetonitrile at 100 μM concentration (unless otherwise stated) for each reagent. Similar mass spectra were obtained for reaction mixtures prepared at higher concentrations (up to 500 μM) and in different solvents such as methanol, methanol−water, and ethyl acetate, as well as in their acidified solutions with formic acid. Concentrations higher than 500 μM were not employed to prevent contaminations of MS instruments.

Materials and Reagents. Acetonylacetone (97%), benzaldehyde (99%), *n*-butylamine (99.5%), cyclohexanone (99%), ethanolamine (98%), phenylhydrazine (97%), 2,4,6-triphenylpyrylium tetrafluoroborate (98%), and screw-top glass vials with 9 mm screw-thread neck and 100 μL glass microvial/insert were all purchased from Sigma-Aldrich (St. Louis, MO, USA). Aniline (99.8%) was provided by Acros Organics (Geel, Belgium). Chlorophenylhydrazine was obtained from Santa Cruz Biotechnology (Dallas, TX, USA). Bromophenylhydrazine (98%) was supplied by Syntonix Pharmaceuticals (Waltham, MA, USA). Nitrophenylhydrazine was bought from Chem Service (West Chester, PA, USA). Pentylhydrazine (95%) was provided by Combi-Blocks (San Diego, CA, United States). 2-Butanone was acquired from Fisher Scientific (Pittsburgh, PA, USA).

https://dx.doi.org/10.1021/acs.analchem.0c02960
Anal. Chem. 2020, 92, 15025−15033

Scheme 1. Uncatalyzed Gas-Phase B-D Cyclization Reaction between Cyclohexanone (*1*) and Phenylhydrazine (*2*)

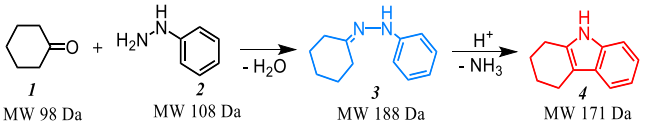

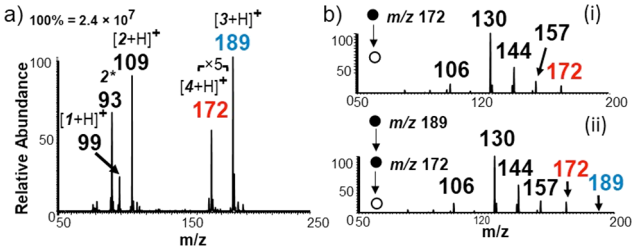

Figure 2. Positive ion mode mass spectrum of the B-D cyclization showing (a) full MS analysis and (b) MS^2 product ion scan at (i) m/z 172 and MS^3 spectrum of m/z 172 derived from the MS^2 of (ii) m/z 189. *$[2 + H-NH_2]^{\cdot+}$ species at m/z 93.

RESULTS AND DISCUSSION

Gas-Phase Borsche−Drecsel Cyclization. Motivated by our desire to differentiate closely related organic compounds through the high-throughput gas-phase reaction screening, we started our investigation with Borsche−Drecsel (B-D) cyclization. The conventional solution-phase B-D cyclization reaction (Scheme 1) is achieved by heating the reaction mixture (i.e., hydrazine and ketone) in the presence of concentrated hydrochloric acid.[34,35] In our experiment, headspace vapors of cyclohexanone ***1*** (MW, 98) and phenylhydrazine ***2*** (MW, 108) were simply brought in close proximity and ionized by the contained-APCI source. The results of this experiment are shown in Figure 2a, where the expected cyclization product ***4*** was observed at m/z 172 immediately upon the application of DC voltage. The protonated form of the initial condensation product, cyclohexanone phenylhydrazone **3**, was also observed at m/z 189, alongside the unreacted reagents ***1*** and ***2*** at m/z 99 and 109, respectively. The identity of the cyclization product ***4*** was confirmed by MS/MS experiment (Figure 2b-i), which showed fragment ions at m/z 144 and 130 via the loss of ethylene and propene, respectively. These fragment ions are consistent with the fragmentation pattern observed for protonated tetrahydrocabazole (***4***) generated in the gas phase (under vacuum) through multiple stage (MS^3) fragmentation of m/z 189 to give m/z 172 (Figure 2b-ii). The correspondent MS^2 fragmentation pattern of m/z 189 is provided in the Supporting Information (Figure S1). Moreover, the identities of reaction products and intermediates were further proved by high-resolution (Orbitrap MS) experiments that provided −4.0 and −4.5 ppm mass accuracy for compounds ***3*** and ***4***, respectively. The successful implementation of gas-phase B-D cyclization under the contained-APCI experimental condition indicates that the ionizing particles are highly acidic in nature, suggesting the presence of low molecular weight protonated water clusters $[H^+(H_2O)_n; n = 1, \text{or } 2]$.[36,37] The fact that expected products are detected without heating also suggests that reactants are activated by the collision events in the plasma. The energy deposited is sufficient to break the N−N bond in the hydrazine, resulting in the release of amino phenyl radical species, which was detected at m/z 93 (Figure 2a). Although this species is not directly involved in the B-D cyclization reaction, its presence indicates high energy collisions (energy ≥2.6 eV for N−N bonds in hydrazines)[38] in the corona discharge upon the application of ≥4 kV DC voltage). No ion signal corresponding to reactants and products was observed in the absence of applied DC voltage. To evaluate solvent effects, the same reaction was conducted in solution-phase (reagent concentrations ≤500 μM), which was subsequently compared to the reactivity of charged microdroplets derived from electrospray ionization. All experiments were performed without the addition of external acid. As expected, cyclization product ***4*** was not formed, even at higher MS inlet temperatures (Figure S2). Acidification also did not provide any improvements in the charged microdroplet reaction condition under the concentrations tested (data is not shown); this is perhaps due to the need to properly tune pH and solvent properties. This interpretation is consistent with a recent study, which required 1 M methanolic HCl to be added to the reaction mixture (in the presence of 0.1 M phenylhydrazine) before droplet reactions[39] were initiated in the electrospray process.

Solvent-Free Katritzky Chemistry. Gas-phase version of Katritzky chemistry[40−42] involving pyrylium cation (***5***) and ethanolamine (***6***) was also investigated in the absence of heat and solvent (Scheme 2). In this case, the type of product formed was strongly dependent on the magnitude of the applied DC voltage. For example, only the pyrylium cation (nonvolatile solid sample, estimated vapor pressure, VP ≈ 1.9 × 10^{-7} kPa)[43] was detected in high abundance at m/z 309 (Figure 3b) when no DC voltage was applied, indicating gas-phase reaction between ***5*** and ***6*** did not occur. An obvious new peak appeared at m/z 308 (***8***) upon the application of 4 kV DC potential (Figure 3c); this marked the onset of microplasma formation (see insert, Figure 3c for the dependence of m/z 308 signal on applied voltage). We confirmed that ***8*** is not produced by hydride elimination from ***5*** since no such peak was observed in the absence of ***6***. Instead, the conversion of the pyrylium cationinto the corresponding pyridinium cation occurred via reaction with ethanolamine vapor to give **7**, which spontaneously decomposed by losing ethylene oxide (MW, 44 Da) to yield ***8***. This spontaneous decomposition is not surprising given the reactive nature of the contained-APCI source. In this case, the presence of the nonmobile permanent charge on the quaternary ammonium nitrogen atom in **7** drives the loss of neutral ethylene oxide.

Scheme 2. Solvent-free Katritzky Chemistry Involving 2,4,6-Triphenylpyrylium Cation (*5*) and Ethanolamine (*6*) under Contained-APCI Reaction Condition

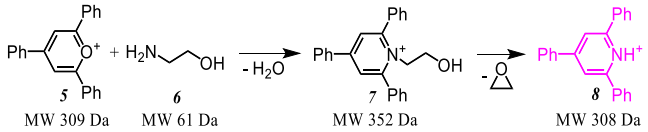

To further explore the full spectrum of chemistry occurring in this gas-phase Katritzky transamination reaction, we increased the applied voltage from 4 to 6 kV, expecting a concomitant increase in the concentration of active species (e.g., electron density) present in the corona discharge. As anticipated, two additional reaction products were observed at m/z 327 and 388 under this intense plasma condition (Figure 3d), which provided valuable insight into the reaction

https://dx.doi.org/10.1021/acs.analchem.0c02960
Anal. Chem. 2020, 92, 15025−15033

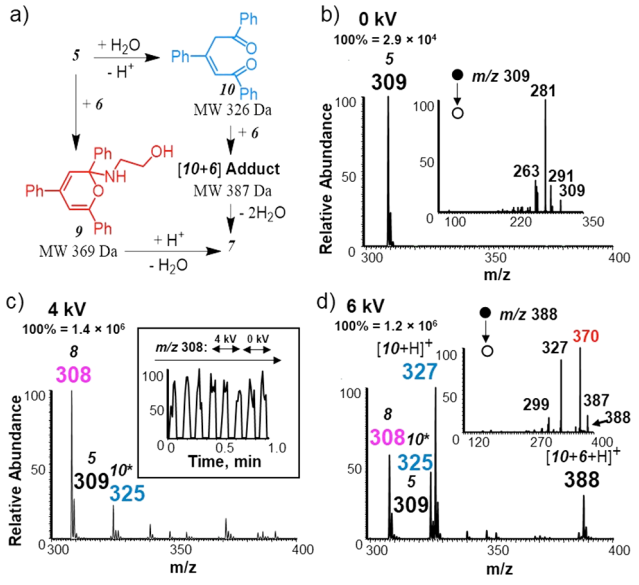

Figure 3. (a) Schematic showing the proposed pathway for gas phase Katritzky reaction involving 2,4,6-triphenylpyrylium cation and ethanolamine. Positive-ion mass spectra recorded at (b) 0 kV, (c) 4 kV, and (d) 6 kV. Insert in (c) shows extracted ion chronogram at *m/z* 308 (final product ***8***), indicating dependence of reaction on applied DC voltage. Inserts in (b, d) show MS^2 spectra of reaction products *m/z* 309 and *m/z* 388, respectively. *$[\boldsymbol{10}-H]^+$ species at *m/z* 325.

mechanism. The reaction between ***5*** and an amine is known to proceed via two stable intermediates: (i) the pseudobase intermediate (***10***, Figure 3a) is formed from a direct interaction between water and ***5***. Subsequent reaction between ***10*** and the amine proceeds to give the final pyridinium product ***7*** after losing two water molecules, and (ii) 2H-pyran intermediate (***9***), which is formed through a direct reaction between ***5*** and ***6***. The conspicuous absence of the stable 2H-pyran intermediate at *m/z* 370 (Figure 3d) rules out this pathway, which is consistent with previously reported solvent-limited Katritzky chemistry.[44,45] Instead, reaction pathway involving the pseudobase intermediate is clearly evident in the detection of ion signals at *m/z* 327 and 388, which represent the protonated and ethanolamine adducts of ***10***, respectively. Multiple-stage tandem MS experiments confirmed that these two intermediates are related in that the adduct at *m/z* 388 dissociated to give *m/z* 327 (insert, Figure 3d), which in turn produced fragmentation pattern in MS^3 that was similar to the MS^2 product ion spectrum generated from the pseudobase ***10*** (Figure S3). The identity of all observed reaction products was confirmed by high-sresolution data (mass accuracy: 1.3 ppm for ***8***, 0.04 ppm for ***9***, 1.9 ppm for ***10***, and 1.9 ppm for [***10*** + ***6***] adduct). For the purposes of comparison, we performed bulk-solution Katritzky reaction, which showed the existence of the 2H-pyran intermediate ***9*** and final product ***7***, within <3 min of reaction time using excess ethanolamine (Figure S4). The pseudobase intermediate ***10*** and the decomposition product ***8*** were completely absent in the solution-phase reaction, again confirming a different pathways for the gas-phase atmospheric pressure Katritzky chemistry.

pH and amine basicity are known to influence the efficiency of bulk solution-phase Katritzky reactions.[46] To investigate if similar effect will exist in the gas-phase, we replaced ethanolamine (VP, 64 Pa; gas-phase basicity, 896.8 kJ/mol) with *n*-butylamine (VP 9 kPa; gas-phase basicity, 886.6 kJ/mol) in a gas-phase reaction with 2,4,6-triphenylpyrylium cation at 6 kV. Despite the marked difference in vapor pressure (>100× in favor of *n*-butylamine), we observed significant decrease in reaction efficiency when *n*-butylamine vapor was reacted with the pyrylium cation under this intense plasma reaction condition. In particular, while pyrylium to pyridinium conversion still occurred in real time (Scheme S1, Figure S5), detectable ion signals related to the pseudobase intermediate, ***10***, [e.g., *m/z* 325 $(M-H)^+$, 327 $(M + H)^+$, and 400 (M + *n*-butylamine + $H)^+$] were not observed. This result clearly demonstrates that the contained-APCI reaction screening platform is sensitive to subtle changes in a chemical environment and that its operation is not solely governed by activation via electron collisions. In this case, the opening of the ring in the pyrylium cation to form the di-ketone pseudobase intermediate is found to be affected by the presence of different primary amines, an effect that is also observed in solution phase[47] and thus confirming distinct mechanisms can be activated under different reaction conditions.

Gas-Phase Paal–Knorr Pyrrole Synthesis. The realization that primary amines can react favorably with the di-ketone functionality (e.g., as in the pseudobase intermediate ***10***) in the gas-phase led us to further investigate solvent-free Paal–Knorr pyrrole synthesis (Scheme 3 and Figure S6) using the new contained-APCI platform. The Paal–Knorr pyrrole synthesis is a very valuable synthetic method for obtaining substituted furans and pyrroles, which are common structural components of many natural products. The importance of this reaction is exemplified by the numerous methodologies developed to improve yield through the use of greener reaction conditions, including the use of micellar systems in water,[48] ionic liquids,[49] microwave heating,[50] and ultrasound.[51] We envisioned that charged microdroplets derived from electrospray[52,53] may also represent another green media for the Paal–Knorr pyrrole synthesis but all attempts failed to yield expected reaction products under this confined volume droplet condition (Scheme S2 and Figure S7). We then performed the reaction under solvent-free conditions using headspace vapors of acetonylacetone (***11***) and *n*-butylamine (***12***) in the presence of corona discharge. We observed high abundance of the Schiff's base *13* at *m/z* 170 and the final cyclized pyrrole product *14* (*m/z* 152) immediately after applying 6 kV of DC voltage (Figure 4a). Here too, the final product structure was confirmed by MS/MS (Figure 4b-i and Figure S6), high-resolution Orbitrap analysis (mass tolerance 0.4 ppm), and via the analysis of standard 1-butyl-2,5-dimethyl-1H-pyrrole compound, which showed the identical MS/MS fragmentation pattern (Figure 4b-ii). The fact that two molecules of *n*-butylamine do not attack acetonylacetone to react with the individual ketone groups separately indicates that the cyclization step following the formation of the Schiff's base is fast. Similar product distribution was recorded when ethanolamine was used to react with acetonylacetone in gas phase (Figures S7 and S8). Here, we observed improved reaction efficiency in accordance with increased gas-phase basicity for ethanolamine compared with *n*-butylamine. The Schiff's base (*m/z* 158) as well as the cyclized pyrrole (*m/z* 140) reaction products were detected at 3.6 and 3.9 ppm mass accuracies, respectively, and further characterized by MS/MS. It is important to note that stable cyclization products were detected in the gas-phase Paal–Knorr pyrrole synthesis without any decomposition. This is contrary to the

https://dx.doi.org/10.1021/acs.analchem.0c02960
Anal. Chem. 2020, 92, 15025–15033

corresponding gas-phase version of Katritzky reaction where the presence of the permanent positive charge on the cyclized pyridinium cation facilitated product decomposition. This insight reaffirms the contained-APCI MS reaction screening platform is sensitive to the chemical structure, and that the observed product distribution is not a mere result of harsh ionization conditions. For example, when phenylhydrazine vapor (as opposed to primary amine) was exposed to acetonylacetone, the reaction is stopped at Schiff's base formation without subsequent cyclization (Scheme S3 and Figure S9). Just like the charged micropdroplet environment failed to yield expected products in the absence of catalyst, bulk solution-phase reaction also did not afford detectable cyclization products for all reactants tested.

Scheme 3. Paal–Knorr Pyrrole Synthesis from Acetonylacetone (*11*) and *n*-Butylamine (*12*) Using the Gas-Phase Contained-APCI Reaction Screening Platform

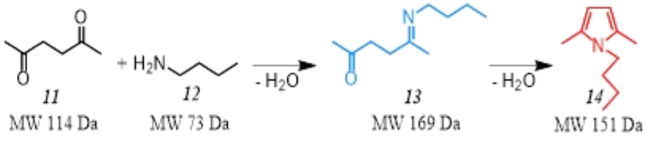

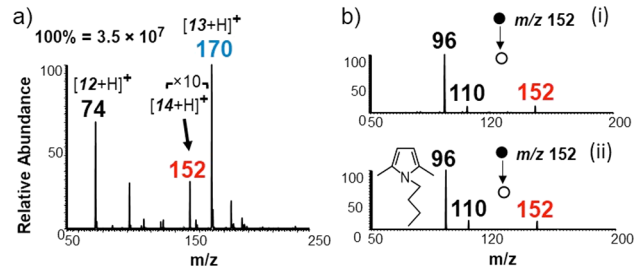

Figure 4. (a) Positive ion mode full mass spectrum for Paal–Knorr reaction recorded after exposing *11* and *12* headspace vapors to corona discharge. (b) Comparison of MS^2 spectra of gas-phase reaction product *14* produced in (a) at (i) *m*/*z* 152 with MS/MS of (ii) standard 1-butyl-2,5-dimethyl-1H-pyrrole.

Gas-Phase Radical-Mediated Coupling of Hydrazines to Give Secondary Amines. During the screening process, we observed a unique radical chemistry involving hydrazines that occurred only in the absence of a second reactant. Free radical formation from hydrazines is not uncommon,[54,55] it can result from both one- and two-electron oxidations reactions. However, the subsequent coupling chemistry that we have observed (Scheme 4) yielding secondary amines has not been reported before. This uncatalyzed plasma-mediated amine synthesis via the formation of free radicals from hydrazine is applicable to both aromatic and aliphatic compounds, indicating that it could represent a facile route to synthesize secondary amines, which are extremely important pharmacophores in numerous physiological activities.[56] In a typical experiment, headspace vapor of different hydrazines (aliphatic and aromatic) were exposed to corona discharge at 6 kV. All hydrazines followed the mechanism illustrated in Scheme 4, in which the N–N and C–N bonds were cleaved homolytically to form R–NH$^{\cdot}$ (*16*) and R$^{\cdot}$ (*17*) radicals, respectively, which subsequently reacted to give the final coupling product (*18*). An example is shown in Figure 5a demonstrating the formation of protonated radical *16* (*m*/*z* 93) and protonated final product *18a* (diphenylamine, *m*/*z* 170) due to coupling reaction between the two radical intermediates. Figure 5b shows a comparison of the MS/MS product ion spectrum for synthesized diphenylamine product (*18a*, Figure 5b-i) to the MS/MS spectrum derived from a standard diphenylamine compound (Figure 5b-ii). As can be observed, the two spectra are identical proving the structure of *18a*. The identity of the gas-phase product *18a* from phenylhydrazine (*15a*) was confirmed by exact mass measurements where we recorded 0.02 ppm mass accuracy. Aside from phenylhydrazine, other aromatic hydrazines have shown the same type of radical chemistry when exposed to plasma under the contained-APCI reaction condition, even when the polarity of the discharge voltage was changed from positive to negative.

Scheme 4. Uncatalyzed Conversion of aromatic phenylhydrazine derives in radical-mediated plasma chemistry[a]

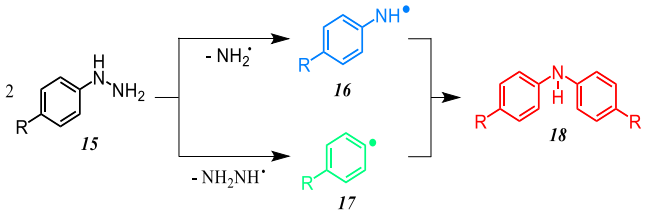

[a]Note that R = H (*15a*, *18a*), R = Cl (*15b*, *18b*), R = Br (*15c*, *18c*), and R = NO_2 (*15d*, *18d*)

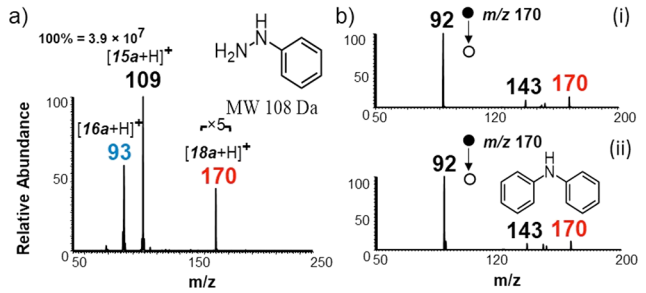

Figure 5. (a) Positive ion mode mass spectrum recorded after exposure of phenylhydrazine headspace vapor to corona discharge. (b) CID product ion mass spectra for (i) atmospheric pressure coupling product *18a* in (a) and (ii) standard diphenylamine at *m*/*z* 170.

For instance, Figure S10a shows the negative-ion mode mass spectrum recorded when *p*-chlorophenylhydrazine (MW, 143 Da) was exposed to corona discharge generated by negative DC voltage (−5 kV). The spectrum shows the presence of radical anions M$^{\cdot-}$ and (M−NH_2)$^{\cdot-}$ at *m*/*z* 143 and 127, respectively, alongside the expected coupling product as deprotonated (M−H)$^-$ and hydrated (M−H + H_2O)$^-$ species at *m*/*z* 237 and 255, respectively. The insert in Figure S10a shows the isotopic distribution of the hydrated product ion, which matches expected pattern for a compound containing two chlorine atoms. Figure S10b represents the positive ion mode mass spectrum recorded after exposure of pentylhydrazine vapor to corona discharge, which showed the production of a coupled product at *m*/*z* 158 in high abundance from this aliphatic hydrazine. An unexpected NH adduct (*m*/*z* 173, Figure S10b) was also observed. Other hydrazines tested include *p*-bromophenylhydrazine and *p*-nitrophenylhydrazine;

https://dx.doi.org/10.1021/acs.analchem.0c02960
Anal. Chem. 2020, 92, 15025−15033

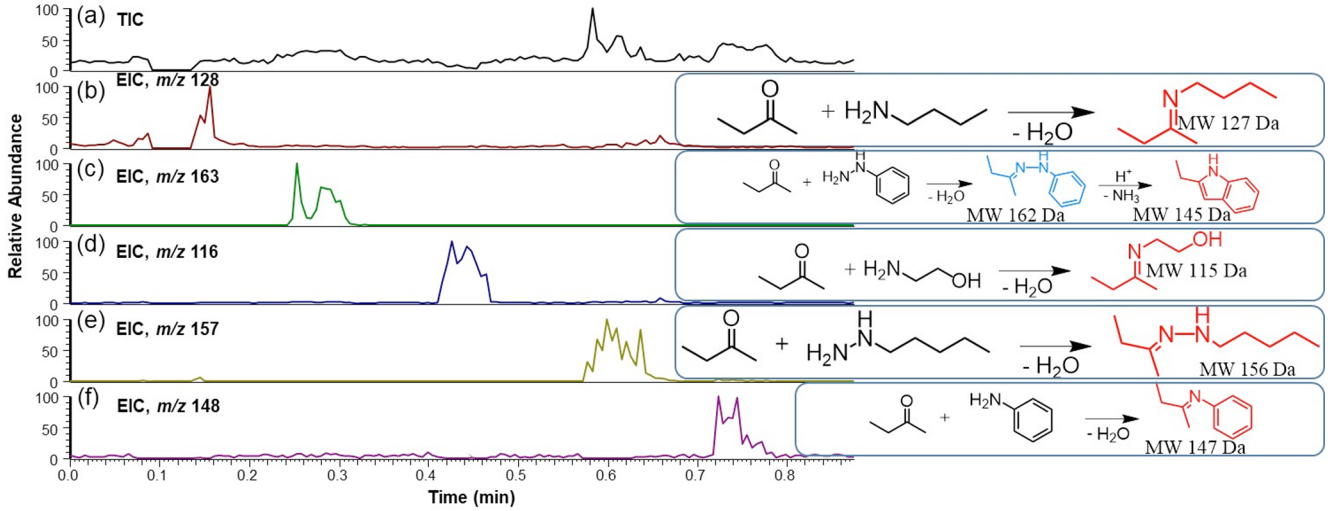

Figure 6. (a) Total ion chromatogram, TIC, and (b–f) extracted ion chronograms (XIC) of high-throughput screening involving reaction of 2-butanone with (b) butylamine (product *m/z* 128), (c) phenylhydrazine (product *m/z* 163), (d) ethanolamine (product *m/z* 116), (e) pentylhydrazine (product *m/z* 157), and (f) aniline (product *m/z* 148). Reaction time was kept at 5 s per sample, followed by another 5 s waiting time to limit carryover issues.

these were analyzed in positive and negative ion modes and showed the expected coupling products (Figures S11–S13).

High-Throughput Experimentation. Thus far, we have discussed the gas-phase versions of B-D cyclization, Katritzky chemistry, Paal–Knorr pyrrole synthesis, and the novel radical mediated hydrazine coupling reaction and observed the expected solution-phase reaction product without the use of a catalyst. As already alluded to, the underlying objective for studying these reactions is the creation of high-throughput gas-phase screening platform for the differentiation of closely related chemical structures. Here, we summarize our findings based on reactions discussed above. Take primary amines and hydrazines as an example. These two very similar functional groups can be easily distinguished simply by exposing the headspace vapors to corona discharge in the contained-APCI MS platform. Hydrazines undergo coupling reactions via radical-mediated mechanism and culminate in the formation of secondary amine, while primary amines form N-alkylation tertiary amine product via carbocation formation (Scheme S4 and Figure S14). Both intermediates (radical vs carbocation) can be detected in real time as well as the distinct products. When reacted with monoketones (cyclohexanone and acetone), primary amines form only the corresponding Schiff's base (Schemes S5–S7and Figures S15–S17), but hydrazines afford both the condensation and cyclization products, always spaced by 17 Da mass difference, indicating the loss of ammonia from the Schiff's base to give the final cyclized product (Figure 2a and Figure S18,S19, and Scheme S8). On the other hand, when exposed to headspace vapors of di-ketone functionality (e.g., acetonylacetone), primary amines cyclized through two sequential losses of water molecules (Figure 4) whereas hydrazines did not (Figure S9). Clearly, these gas-phase reactions also enable aliphatic mono-ketones and di-ketones to be distinguished through reaction with primary amines and hydrazines. Aromatic and aliphatic hydrazines can be distinguished via gas-phase B-D cyclization; aromatic hydrazines cyclized when exposed to vapors of monoketones but aliphatic hydrazine did not. Hydrazines did not react with the pyrylium cation in gas-phase Katritzky chemistry, providing a means to differentiate aliphatic amines from aliphatic hydrazines although the two compounds react with the carbonyl functional group to form the corresponding imine.

To demonstrate the high-throughput capabilities of this new contained-APCI MS screening platform, we tested the reactivity of five different compounds (*n*-butylamine, phenylhydrazine, ethanolamine, pentylhydrazine, and aniline), separately toward 2-butanone vapor in real time. Exposure time for each reagent was kept at 5 s, followed by another 5 s delay time yielding a total of 10 s interval between reactants, which was found optimal to limit carryover effect. No significant carryover effect was observed for all 13 chemical reagents tested. The noncontact nature of the contained-APCI platform also aids in limiting contamination.[24] Therefore, the reactivity of all five reagents could be screened in under 60 s. The results of this experiment are summarized in Figure 6 and Figure S20, which show clean product formation for each reactant without interference from previously analyzed reagents. While this experiment attempts to differentiate amines from hydrazines using their reaction with 2-butanone, it can be observed that the majority of the reactants form similar product, making functional group identification challenging. This issue can be addressed through the implementation of other reactions in parallel. Here is where the high-throughput experimentation capabilities of the contained-APCI MS platform can be realized. In this respect, the experimental setup described in Figure 1 having three inputs is not intended for three component reaction screening. Instead, the three inputs are proposed to allow a given analyte (reagent B, Figure 1) to be interrogated by two different reagents (A and C) in parallel. For example, both aniline and phenylhydrazine reagents react individually with 2-butanone to give the corresponding Schiff's base via the loss of a water molecule. By replacing the 2-butanone analyte with pyrylium cation, only the amine is expected to react to produce the corresponding pyridinium cation as demonstrated in Figure S21. By combining this high-throughput experimentation procedure with tandem MS, it should be possible to obtain complete structural information in a matter of seconds, something that could be useful for structural discriminations

https://dx.doi.org/10.1021/acs.analchem.0c02960
Anal. Chem. 2020, 92, 15025–15033

in situations where high-resolution instruments are not available. The process can be accomplished manually or via a robotic arm. Analytically, the ability to perform this experiment manually will be advantageous in field applications (i.e., on-site analysis) for complex mixture analysis, where the front end reactions can produce a shift in mass for the analyte, thereby providing more confidence for MS/MS experiments conducted without prior separation.

CONCLUSIONS

In summary, we have introduced a new contained-APCI MS reaction screening platform to monitor gas-phase reactions at atmospheric pressure in real time using headspace vapors. We demonstrated that solution-phase reaction products expected from B-D cyclization, Katritzky chemistry, and Paal−Knorr pyrrole synthesis could be formed in the gas-phase without the use of a catalyst. This suggested that the nonequilibrium plasma chemistry employed in the contained-APCI platform is chemically selective, enabling closely related functional groups (e.g., amines and hydrazine) to be distinguished in a high-throughput fashion. The contained-APCI MS screening platform also enabled the discovery of a novel radical-mediate hydrazine coupling reaction in the gas-phase for the synthesis of aliphatic and aromatic secondary amines. The absence of solvent and effective electron collisions in the ambient corona discharge offered increased reaction efficiency for the gas-phase, compared with the corresponding reactions performed under bulk solution-phase and charged microdroplet reaction conditions. The simplicity, low sample consumption, and the speed of this high-throughput experimentation involving gas-phase reaction screening, occurring without heat, solvent, catalyst, and nebulizing gas, and the possibility of studying the reactivity of nonvolatile organic compounds under solvent-free environment give these findings potential to have significant impact in drug discovery as well as in new reaction discovery.

ASSOCIATED CONTENT

Supporting Information

The Supporting Information is available free of charge at https://pubs.acs.org/doi/10.1021/acs.analchem.0c02960.

Tandem MS analysis of product **3** from B-D cyclization reaction; B-D cyclization reaction for bulk, droplet, and gas phases; fragmentation of the pseudobase, pyrylium/pseudobase adduct, and pyridinium cation for Katritzky reaction; Katritzky reaction, and kinetics in bulk conditions; reaction of 2,4,6-triphenylpyrylium cation and *n*-butylamine; tandem MS fragmentation patterns for Paal−Knorr synthesis; analysis of acetonylacetone/ethanolamine reaction; interaction between acetonylacetone and phenylhydrazine; radical coupling of hydrazines; N-alkylation of amines; interaction between cyclohexanone and aniline; reaction of cyclohexanone with ethanolamine; interaction of 2-butanone with ethanolamine; analysis of 2-butanone/phenylhydrazine reaction mixture; high-throughput experimentation; and references (PDF)

AUTHOR INFORMATION

Corresponding Author

Abraham K. Badu-Tawiah − *Department of Chemistry and Biochemistry, The Ohio State University, Columbus, Ohio 43210, United States;* orcid.org/0000-0001-8642-3431; Email: badu-tawiah.1@osu.edu

Authors

Dmytro S. Kulyk − *Department of Chemistry and Biochemistry, The Ohio State University, Columbus, Ohio 43210, United States*

Enoch Amoah − *Department of Chemistry and Biochemistry, The Ohio State University, Columbus, Ohio 43210, United States*

Complete contact information is available at: https://pubs.acs.org/10.1021/acs.analchem.0c02960

Author Contributions

The manuscript was written through contributions of all authors. All authors have given approval to the final version of the manuscript.

Notes

The authors declare no competing financial interest.

ACKNOWLEDGMENTS

This work was supported by National Science Foundation (award no. CHE-1900271) and the U.S. Department of Energy, Office of Science, Office of Basic Energy Sciences, Condensed Phase and Interfacial Molecular Science (award no. DE-SC0016044).

REFERENCES

(1) Inglese, J.; Johnson, R. L.; Simeonov, A.; Xia, M.; Zheng, W.; Austin, C. P.; Auld, D. S. *Nat. Chem. Biol.* **2007**, *3*, 466−479.
(2) Montgomery, J. *Science* **2011**, *333*, 1387−1388.
(3) Sun, S.; Kennedy, R. T. *Anal. Chem.* **2014**, *86*, 9309−9314.
(4) Wleklinski, M.; Loren, B. P.; Ferreira, C. R.; Jaman, Z.; Avramova, L.; Sobreira, T. J. P.; Thompson, D. H.; Cooks, R. G. *Chem. Sci.* **2018**, *9*, 1647−1653.
(5) Loren, B. P.; Ewan, H. S.; Avramova, L.; Ferreira, C. R.; Sobreira, T. J. P.; Yammine, K.; Liao, H.; Cooks, R. G.; Thompson, D. H. *Sci. Rep.* **2019**, *9*, 14745.
(6) Girod, M.; Moyano, E.; Campbell, D. I.; Cooks, R. G. *Chem. Sci.* **2011**, *2*, 501−510.
(7) Banerjee, S.; Zare, R. N. *Angew. Chem., Int. Ed.* **2015**, *54*, 14795−14799.
(8) Badu-Tawiah, A. K.; Li, A.; Jjunju, F. P. M.; Cooks, R. G. *Angew. Chem., Int. Ed.* **2012**, *51*, 9417−9421.
(9) Lee, J. K.; Samanta, D.; Nam, H. G.; Zare, R. N. *Nat. Commun.* **2018**, *9*, 1562.
(10) Picotti, P.; Aebersold, R. *Nat. Methods* **2012**, *9*, 555−566.
(11) Zhao, Y.; Riley, N. M.; Sun, L.; Hebert, A. S.; Yan, X.; Westphall, M. S.; Rush, M. J. P.; Zhu, G.; Champion, M. M.; Medie, F. M.; DiGiuseppe Champion, P. A.; Coon, J. J.; Dovichi, N. J. *Anal. Chem.* **2015**, *87*, 5422−5429.
(12) Fornelli, L.; Durbin, K. R.; Fellers, R. T.; Early, B. P.; Greer, J. B.; LeDuc, R. D.; Compton, P. D.; Kelleher, N. L. *J. Proteome Res.* **2017**, *16*, 609−618.
(13) Park, J.; Piehowski, P. D.; Wilkins, C.; Zhou, M.; Mendoza, J.; Fujimoto, G. M.; Gibbons, B. C.; Shaw, J. B.; Shen, Y.; Shukla, A. K.; Moore, R. J.; Liu, T.; Petyuk, V. A.; Tolić, N.; Paša-Tolić, L.; Smith, R. D.; Payne, S. H.; Kim, S. *Nat. Methods* **2017**, *14*, 909−914.
(14) Foreman, D. J.; McLuckey, S. A. *Anal. Chem.* **2020**, *92*, 252−266.
(15) Poad, B. L.; Pham, H. T.; Thomas, M. C.; Nealon, J. R.; Campbell, J. L.; Mitchell, T. W.; Blanksby, S. J. *J. Am. Soc. Mass Spectrom.* **2010**, *21*, 1989−1999.
(16) Marshall, D. L.; Pham, H. T.; Bhujel, M.; Chin, J. S. R.; Yew, J. Y.; Mori, K.; Mitchell, T. W.; Blanksby, S. J. *Anal. Chem.* **2016**, *88*, 2685−2692.

(17) Sheng, H.; Tang, W.; Yerabolu, R.; Max, J.; Kotha, R. R.; Riedeman, J. S.; Nash, J. J.; Zhang, M.; Kenttämaa, H. I. *J. Org. Chem.* **2016**, *81*, 575−586.
(18) Cernak, T. *Chem* **2016**, *1*, 6−9.
(19) Jeffries-El, M.; Sauvé, G.; McCullough, R. D. *Macromolecules* **2005**, *38*, 10346−10352.
(20) Xie, Y.; He, L.-F.; Lin, S.-C.; Su, H.-F.; Xie, S.-Y.; Huang, R.-B.; Zheng, L.-S. *J. Am. Soc. Mass Spectrom.* **2011**, *20*, 2087−2092.
(21) Papanastasiou, M.; McMahon, A. W.; Allen, N. S.; Johnson, B. W.; Keck-Antoine, K.; Santos, L.; Neumann, M. G. *Int. J. Mass Spectrom.* **2008**, *275*, 45−54.
(22) Cabrera-Pardo, J. R.; Chai, D. I.; Liu, S.; Mrksich, M.; Kozmin, S. A. *Nat. Chem.* **2013**, *5*, 423−427.
(23) Zhang, W.; Huang, G. *Rapid Commun. Mass Spectrom.* **2015**, *29*, 1947−1953.
(24) Kulyk, D. S.; Sahraeian, T.; Wan, Q.; Badu-Tawiah, A. K. *Anal. Chem.* **2019**, *91*, 6790−6799.
(25) Kulyk, D. S.; Swiner, D. J.; Sahraeian, T.; Badu-Tawiah, A. K. *Anal. Chem.* **2019**, *91*, 11562−11568.
(26) Kortshagen, U. R.; Sankaran, R. M.; Pereira, R. N.; Girshick, S. L.; Wu, J. J.; Aydil, E. S. *Chem. Rev.* **2016**, *116*, 11061−11127.
(27) Wang, A.; Qin, M.; Guan, J.; Wang, L.; Guo, H.; Li, X.; Wang, Y.; Prins, R.; Hu, Y. *Angew. Chem., Int. Ed.* **2008**, *47*, 6052−6054.
(28) Yi, Y.; Zhou, J.; Guo, H.; Zhao, J.; Su, J.; Wang, L.; Wang, X.; Gong, W. *Angew. Chem., Int. Ed.* **2013**, *52*, 8446−8449.
(29) Chen, S.; Wan, Q.; Badu-Tawiah, A. K. *Angew. Chem., Int. Ed.* **2016**, *128*, 9491−9495.
(30) Jayaraj, S.; Badu-Tawiah, A. K. *Sci. Rep.* **2019**, *9*, 11280.
(31) Jin, C.; Viidanoja, J.; Li, M.; Zhang, Y.; Ikonen, E.; Root, A.; Romanczyk, M.; Manheim, J.; Dziekonski, E.; Kenttämaa, H. I. *Anal. Chem.* **2016**, *88*, 10592−10598.
(32) Ding, X.; Duan, Y. *Mass. Spectrom. Rev.* **2015**, *34*, 449−473.
(33) Smoluch, M.; Mielczarek, P.; Silberring, J. *Mass. Spectrom. Rev.* **2016**, *35*, 22−34.
(34) Drechsel, E. *J. Prakt. Chem.* **1858**, *38*, 69.
(35) Borsche, W. *Justus Liebigs Ann. Chem.* **1908**, *359*, 49−80.
(36) Sekimoto, K.; Takayama, M. *J. Inst. Electrostat. Jpn.* **2009**, *33*, 38−42.
(37) Sekimoto, K.; Takayama, M. *Eur. Phys. J. D* **2010**, *60*, 589−599.
(38) Szwarc, M. *Proc. R. Soc., A* **1949**, *198*, 267−284.
(39) Marsh, B. M.; Iyer, K.; Cooks, R. G. *J. Am. Soc. Mass Spectrom.* **2019**, *30*, 2022−2030.
(40) Katritzky, A. R.; Mokrosz, J. L.; De Rose, M. J. *Chem. Soc. Perkin Trans. 2* **1984**, *5*, 849−855.
(41) Katritzky, A. R.; Marson, C. M. *Angew. Chem., Int. Ed.* **1984**, *23*, 420−429.
(42) Badu-Tawiah, A. K.; Wu, C.; Cooks, R. G. *Anal. Chem.* **2011**, *83*, 2648−2654.
(43) *Software for estimating vapor pressures (EPI Suite - Estimation Program Interface v4.11) was provided by United States Environmental Protection Agency*. https://www.epa.gov/tsca-screening-tools/download-epi-suitetm-estimation-program-interface-v411. Accessed February 5, 2020.
(44) Badu-Tawiah, A. K.; Cyriac, J.; Cooks, R. G. *J. Am. Soc. Mass Spectrom.* **2012**, *23*, 842−849.
(45) Sahraeian, T.; Kulyk, D. S.; Badu-Tawiah, A. K. *Langmuir* **2019**, *35*, 14451−14457.
(46) Yan, X.; Augusti, R.; Li, X.; Cooks, R. G. *ChemPlusChem.* **2013**, *78*, 1142−1148.
(47) Katritzky, A. R. *Tetrahedron* **1979**, *36*, 679−699.
(48) Veisi, H.; Azadbakht, R.; Ezadifar, M.; Hemmati, S. *J. Heterocycl. Chem.* **2013**, *50*, E241−E246.
(49) Wang, B.; Gu, Y.; Luo, C.; Yang, T.; Yang, L.; Suo, J. *Tetrahedron Lett.* **2004**, *45*, 3417−3419.
(50) Daştan, A.; Kulkarni, A.; Török, B. *Green Chem.* **2012**, *14*, 17−37.
(51) Satyanarayana, V. S. V.; Sivakumar, A. *Ultrason. Sonochem.* **2011**, *18*, 917−922.
(52) Kulyk, D. S.; Miller, C. F.; Badu-Tawiah, A. K. *Anal. Chem.* **2015**, *87*, 10988−10994.
(53) Miller, C. F.; Kulyk, D. S.; Kim, J. W.; Badu-Tawiah, A. K. *Analyst* **2017**, *142*, 2152−2160.
(54) Kalyanaraman, B.; Sinha, B. K. *Environ. Health Perspect.* **1985**, *64*, 179−184.
(55) Goodwin, D. C.; Aust, S. D.; Grover, T. A. *Chem. Res. Toxicol.* **1996**, *9*, 1333−1339.
(56) Salvatore, R. N.; Yoon, C. H.; Jung, K. W. *Tetrahedron* **2001**, *57*, 7785−7811.

https://dx.doi.org/10.1021/acs.analchem.0c02960
Anal. Chem. 2020, 92, 15025−15033